Comparison of detonation cell size models for alternative fuel blends composed of H_2, CO, CH_4

A. Gupta†, A. Poyet‡, R. Stowe*,
V. Rodriguez‡, A. Chinnayya‡, S. S-M. Lau-Chapdelaine†

† Royal Military College of Canada, Kingston, Ontario, Canada
‡ Institut Pprime, UPR 3346, CNRS, ISAE-ENSMA, Université de Poitiers, France
* Defence Research and Development Canada, Valcartier, Québec, Canada

1 Introduction

The global push for renewable energy has spurred interest in hydrogen power alongside alternative fuels like hydrogen-enriched natural gas (HENG) [1], synthesis gas [2], biogas [3], wood gas, and coal gas [4]. The anaerobic decomposition of energetic materials and the risk of battery fires raises concerns related to the storage of batteries in warehouses and electric vehicles [5], [6]. These blends, comprising hydrogen, methane, carbon monoxide, and carbon dioxide, are commonly used in deflagrative combustion but can detonate under specific conditions, posing risks. In aerospace, rotating detonation engines (RDEs) may offer pressure-gain combustion, promising smaller, cost-effective designs running on alternative fuels, enhancing payload, range, and environmental sustainability. The increasing interest in multi-fuel blends requires a safety analysis of their detonability, with detonation cell size (λ) being a key parameter tied to critical physical dimensions. Factors affecting λ include pressure, mixture composition, equivalence ratio, dilution, and temperature [7]. While existing data primarily covers subatmospheric conditions, industrial applications typically operate at higher pressures. A plot of existing cell size data and ternary fuel applications is shown in Figure 1. This study measures λ for surrogate alternative fuel blends up to initial pressures of 2 bar and compares the results to established models, including scaling by induction length ($\lambda = A\Delta_i$) [8] and pressure dependence; semi-empirical models by Gavrikov *et al.* [9], Ng [10], Monnier *et al.* [11], and Bakalis *et al.* [12] are evaluated, extending predictions to untested conditions.

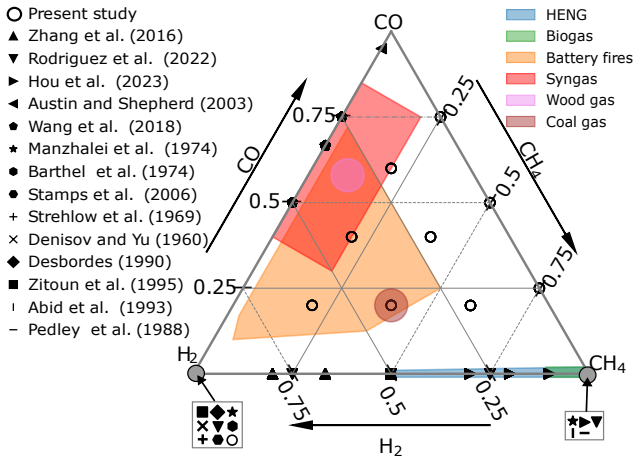

Figure 1: Experimental measurements for multi-fuel mixtures overlaid on alternative fuel applications comprised of H_2, CO, and CH_4; bold numbers correspond to Mix labels in Table 1

2 Experimental Method

Experiments were performed in a 6 m long and 52 mm diameter cylindrical channel (Figure 2). The reactive mixture was ignited by an electrical arc or automotive spark plug. A 1 m Shchelkin spiral

Correspondence to: shem.lau-chapdelaine@rmc.ca

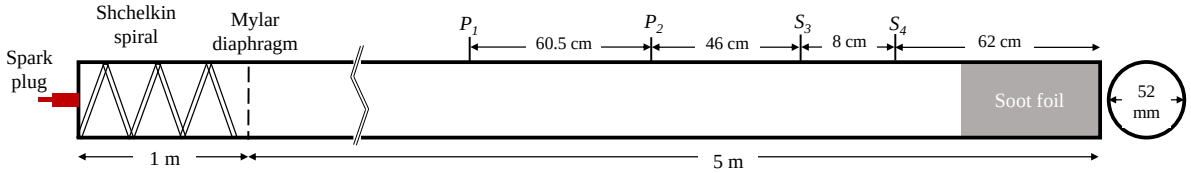

Figure 2: Experimental setup of cylindrical detonation channel at ISAE-ENSMA.

Table 1: Composition by mole fraction of mixtures tested; $X_{f,i} = \frac{X_i}{\sum X_{\text{fuels}}}$

Mix	X_{H_2}	X_{f,H_2}	X_{CH_4}	X_{f,CH_4}	X_{CO}	$X_{f,CO}$	X_{O_2}	Mix	X_{H_2}	X_{f,H_2}	X_{CH_4}	X_{f,CH_4}	X_{CO}	$X_{f,CO}$	X_{O_2}
1	0.083	1/5	0.250	3/5	0.083	1/5	0.583	6	0.095	1/5	0.190	2/5	0.190	2/5	0.524
2	0.190	2/5	0.190	2/5	0.095	1/5	0.524	7	0	0	0.222	1/2	0.222	1/2	0.556
3	0.333	3/5	0.111	1/5	0.111	1/5	0.444	8	0	0	0.133	1/4	0.400	3/4	0.467
4	0.222	2/5	0.111	1/5	0.222	2/5	0.444	9	0	0	0.286	3/4	0.095	1/4	0.619
5	0.111	1/5	0.111	1/5	0.333	3/5	0.444								

promoted deflagration-to-detonation transition (DDT) and the following 3 m provided distance for the detonation to reach steady-state. In the final 2 m, pressure transducers and shock pins were placed to measure the arrival of the detonation and calculate the velocity. A steel soot foil was rolled along the inner circumference of the cylindrical channel in the last 30 cm to record triple point trajectories and to measure cell sizes. In some cases, the spark was not sufficient to obtain a steady detonation in the channel. To promote DDT, a driver mixture of stoichiometric ethylene-oxygen was used, separated by a 60 micron Mylar diaphragm. The mixtures were prepared by partial pressures in a gas cylinder left to mix for 12 hrs; the composition systematically varied mole fractions of hydrogen, carbon monoxide, and methane to effectively model the range of alternative fuel sources. Cell size measurements were recorded for each cell on the foil by taking an average of two authors' measurements. The detonation velocity was obtained by measuring the time between successive peaks in the oscilloscope traces and using the known distances between sensors. These velocities and pressures were compared to expected Champman-Jouguet (CJ) conditions.

3 Results and Discussion

Experiments were performed at initial pressures of 20, 50, 100 and 200 kPa and room temperature. The composition of the multi-fuel mixtures corresponds to the alternative fuels of interest in the ternary plot (Figure 1), the mixtures are shown in Table 1 in mole fraction basis and as a fraction of the fuels where $X_{f,i} = \frac{X_i}{\sum X_{\text{fuels}}}$. Examples of soot foil scans are shown in Figure 3. All tests were within $\pm 2\%$ of the CJ speed for the respective initial pressure, temperature, and mixture composition.

The results for average cell size $\bar{\lambda}$ of each mixture and pressure are listed in Table 2 and indicated by a red dashed line on histograms that show the aggregated distribution of cell sizes measured on the soot foils. Although most databases and papers consider the average cell size as representative of the test, the

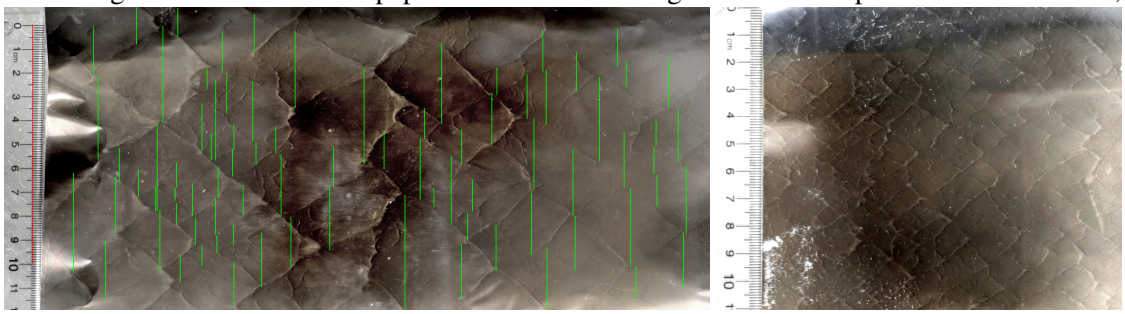

Figure 3: Soot foil for cylindrical channel detonation: Mix 1 ($P_1 = 20.03$ kPa, $T_1 = 17.4$ °C) (left); Mix 1 ($P_1 = 49.90$ kPa, $T_1 = 17.2$ °C) (right). Detonation propagates left to right. Vertical green lines on left foil indicate cell measurements.

histograms expose the variability of cell size on the same foil. Most of the graphs show that most cells are close to the average size; however, some histograms show a right-skewed distribution where most cell size measurements are smaller with several larger cell measurements. In other cases, there are additional smaller peaks at larger cell sizes even when the greatest frequency cell size is smaller. This distribution results from the measurement of smaller cells nested within larger cells as seen in Figure 3. In tests for which a greater number of cells are observed, which is seen in high pressure mixtures, the data tends towards a more normal distribution, resulting in a more representative mean. Trials that had larger cells, for example, at lower pressures, did not have a sufficient sample size to obtain a normal distribution, though an average is still used to compare to models. Although cell size measurements are generally considered accurate within a factor of two [13], analysis of cell distribution on individual soot foils and across trials shows greater variation, which is crucial when developing models to predict cell size.

Table 2: Average cell size and histograms showing the frequency of cell size measurements. Red line: mean; orange line: median.

Mix	20 kPa	50 kPa	100 kPa	200 kPa
1	$\bar{\lambda}$ =33.9 mm	8.5 mm	4.3 mm	2.3 mm
2	28.6 mm	7.4 mm	4.1 mm	2.9 mm
3	17.3 mm	4.4 mm	3.0 mm	no data
4	33.0 mm	7.3 mm	4.2 mm	2.8 mm
5	51.3 mm	12.2 mm	7.1 mm	4.9 mm
6	33.3 mm	11.2 mm	5.4 mm	3.1 mm
7	41.3 mm	14.0 mm	7.7 mm	3.9 mm
8	35.3 mm	45.1 mm	13.6 mm	6.8 mm
9	36.4 mm	10.3 mm	5.0 mm	2.6 mm

3.1 Comparison of cell size models

Several authors have proposed empirical models based on chemical kinetics and thermodynamics to predict the detonation cell size from calculable parameters. Shchelkin and Troshin [8] proposed that the detonation cell size varied linearly with the ZND-based induction zone length ($\bar{\lambda} = A\Delta_\mathrm{i}$), where Δ_i is often defined as the location of maximum temperature gradient behind the leading shock [14]. Gavrikov *et al.* [9] introduced a semi-empirical correlation based on hydrogen-air and hydrogen-air-steam mixtures at different initial temperatures and pressures that used the dimensionless activation energy ($E_\mathrm{a}/RT_\mathrm{vN}$) and a ratio of post-shock temperature to initial temperature (T_vN/T_0). Ng [10] proposed a correlation model based on the induction zone length (Δ_i) and a stability parameter ($\chi = E_\mathrm{a}\Delta_\mathrm{i}/\Delta_\mathrm{r}$) based on hydrocarbon and hydrogen monofuel mixtures from the Caltech database [15] at various initial temperatures, pressures, and equivalence ratios. Recently, Bakalis *et al.* [12] developed an artificial neural network based on CJ Mach number (M_CJ), induction length, and maximum thermicity ($\dot{\sigma}_\mathrm{max}$) which was tested against the various mixtures, test pressures and channel geometries of the Caltech database [15]. They further tested it on untrained data of hydrogen/hydrocarbon/ammonia/nitrous oxide mixtures and compared cell size data from two detonation facilities where it had good agreement [16]. Monnier *et al.* [11] used the premise that the cellular combustion process produces the same burnt mass rate as the steady ZND process, with transverse waves modeled as a stationary ergodic stochastic system. They predicted cell size using graph theory to idealize the cellular structure, geometric prob-

abilities to parameterize the mean burned fraction, and ZND profiles to relate time and position in the reaction zone. They noted that the model depends on the chemical kinetic mechanism used which must be suitable for the mixture. In addition, for the average cell size prediction to be meaningful, the mixture should be regular or moderately irregular and have a high sample size, which is relevant to the distributions seen in this study. It was accurate for mixtures ignited solely by adiabatic shock compression (e.g., H_2, C_3H_8, C_2H_4) but overestimated cell size in CH_4-O_2 due to unaccounted mechanisms like turbulent mixing.

The correlation with induction length to cell size was calculated for the fuel mixtures in Figure 4 at atmospheric temperature and pressure. The corners of the triangle represent mono-fuel mixtures, the edges are binary fuel mixtures, and the central region is ternary fuels, all stoichiometric with oxygen. The coloured contours show a map of the induction length calculated using SDToolBox [21] with the San Diego mechanism [17]; note that $X_{\mathrm{f,CO}} = 1$ is not detonable. The overlaid points are the calculated Shchelkin and Troshin [8] model scaling parameter $\bar{\lambda}/\Delta_i$ for the measured average cell sizes of this study and literature data from various sources. The ratio $\bar{\lambda}/\Delta_i$ generally increases as Δ_i decreases and tends to increase with hydrogen fraction. There were no significant changes in $\bar{\lambda}/\Delta_i$ with change in pressure. Literature estimates $\bar{\lambda}/\Delta_i$ as typically 30 to 70 [13], though the experimental results from this study found some mixtures had lower values for $\bar{\lambda}/\Delta_i$ of 9.6-41.9. There was significant variation for induction length with mechanism when testing San Diego [17], GRI 3.0 [18], Mével *et al.* [19], and Blanquart *et al.* [20]. We did not find a simple relation between fuel quantities and the variation of $\bar{\lambda}/\Delta_i$ in these mixtures and, since the correlation for $\bar{\lambda}/\Delta_i$ is dependent on mixture, estimating the cell size based on induction length alone is not accurate for new mixtures.

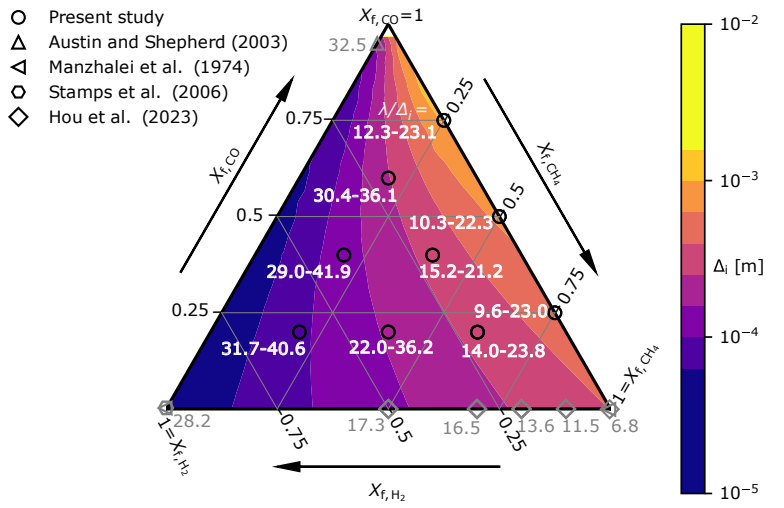

Figure 4: Ternary plot of Δ_i contours and $\bar{\lambda}/\Delta_i$ (notated numbers) of stoichiometric, undiluted methane, hydrogen, carbon monoxide fuel blends at P_1=100 kPa. Ranges indicate variation with mechanism [17]–[20]

The data showed the expected strong correlation of decreasing cell size with increasing pressure following $\bar{\lambda} = aP^b$. Across the various ternary mixtures analyzed, the slopes were fairly consistent in the range of b =-1.42 to -1.26, suggesting a similar dependency of cell size on pressure; however, a =750 to 2800, showing significant variation due to compositional differences.

A limitation of empirical and semi-empirical models is their suitability to parameters outside their fitted dataset, which was typically mono-fuel mixtures. The percentage error between the different prediction models is presented in Figure 5 in a kernel density estimate violin plot for all test mixtures, separated by pressure. The plot shows that the Bakalis *et al.* model [12] has the lowest consistent percentage error between predicted and measured cell sizes, ranging from 5-80%. Monnier *et al.* [11] and Ng [10] were the next most accurate with error mostly in the range 3-200%, and Gavrikov *et al.* [9] showed the most deviation from the measured cell at up to 800% error at 200 kPa. The model accuracy did not appear to be greatly affected by different ternary mixture compositions.

Quantification of the statistical correlation between the tested models and experimental measurements is shown in Table 3. These were done using relative error since cell sizes are concerned with

the ratio to characteristic lengths, like tube diameter. The mean relative error (MRE) measures the sum of all relative error divided by the number of measurements, where a lower value shows less relative error. The root mean squared relative error (RMSRE) presents a similar measure but larger errors have higher weighting. The bias measures systematic error whereby a model consistently deviates from the measured values in one direction. The error-range coverage provides the fraction of model predicted cell sizes which are within the measured cell error for each trial. The absolute error showed heteroscedasticity by presenting a general increase in absolute error with increasing cell size suggesting that the error depends on the magnitude of the measurements. This is because as the cell size increases, the measurements are on the order of millimetres translating to a greater absolute difference, but similar relative difference.

Bakalis *et al.* [12] has the lowest MRE and RMSRE, and the highest error range coverage indicating that the model predicts the cell size measured in this study's tests quite accurately. Monnier *et al.* [11] and Ng [10] had about double the MRE and RMSRE. The three models also have a small difference in MRE and RMSRE showing more consistency in the model throughout the range of parameters tested. They are well within the agreed factor of two deviation for cell size measurements. Gavrikov *et al.* [9] had high errors and bias, and the prediction was not as accurate in the range of cell size measurements. In all models, the resulting error with the experimental mixtures is greater than the reported error in the respective papers, which ranged from 22% [12] to 50% [9].

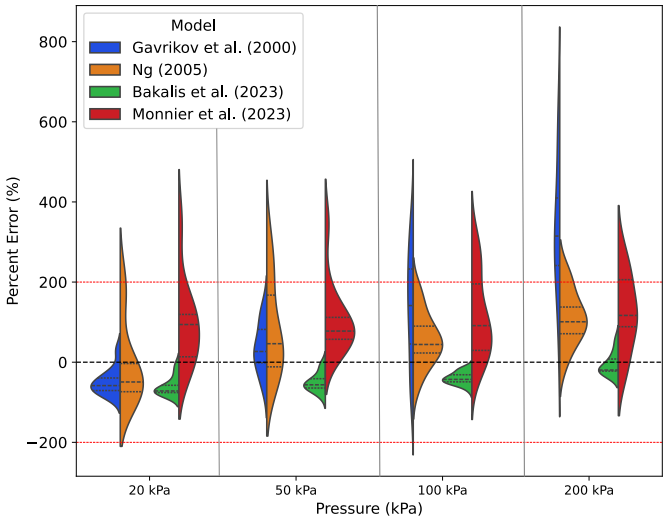

Figure 5: Kernel density estimate plot of model accuracy to experimental results by pressure

Table 3: Statistical correlations between experimental ternary cell sizes and prediction models

Model	MRE	RMSRE	Relative Bias	Error Range Coverage
Bakalis *et al.* [12]	36%	43%	-33%	76%
Gavrikov *et al.* [9]	172%	248%	135%	26%
Ng [10]	89%	118%	58%	65%
Monnier *et al.* [11]	73%	98%	70%	70%

There are several explanations to the discrepancies between cell size model predictions and measured values, as well as between models themselves for these ternary mixtures. First, the input parameters for each required calculation of thermochemical data by the ZND model in SDToolBox [21]. For most calculations, this study used the San Diego mechanism [17], though the $\bar{\lambda}/\Delta_i$ correlation showed to be very sensitive to mechanism. Bakalis and Ng [16] found that their model showed slight differences when using the Mével mechanism compared to the Konnov mechanism the model was trained on. Moreover, some models are more sensitive to initial conditions such as activation energy which can change final predictions for cell size. Thus, the sensitivity of the effective activation energy and induction length due to mechanism leads to a compounding of errors and less repeatable results. Second, the semi-empirical models are fitted for a specific set of initial mixture conditions which are able to model to a relatively low average error. When applying these models to mixtures outside their training data set, such as multi-fuel mixtures, it is uncertain to what extent they are able to accurately predict the cell size,

although they performed well in this case. Third, as seen in Table 2, there is variability to cell size and using an average cell size to represent the test is not always appropriate. To this effect, a wide range of measured cell sizes for a given experiment makes it more difficult to verify a model's suitability to the experiment.

4 Conclusion

This study measured detonation cell sizes for binary and ternary fuel mixtures of H_2, CH_4, CO with stoichiometric O_2 at initial pressures of 20 to 200 kPa in a 52 mm diameter, 6 m long cylindrical channel and compared results to existing prediction models. Steady-state detonation velocity was recorded using pressure transducers and shock pins, while soot foils captured cell size data. Results highlighted significant variability in cell size on a given foil, highlighting the need to consider a distribution rather than a single average value. Comparison with the Shchelkin and Troshin model revealed scaling factors consistent but slightly lower than existing literature $\bar{\lambda}/\Delta_i$ ranges. Monnier *et al.*'s [11] and Bakalis *et al.*'s models [12] demonstrated the highest prediction accuracy across pressures and mixtures tested, though there were discrepancies in all models. These findings provide valuable data for improving cell size prediction models and advancing renewable energy and industrial safety.

References

[1] S. O. Restrepo, J. Denninger, M. Adams, R. Thelen, and A. Adams, "Composition analysis of hydrogen-enriched natural gas by high-pressure benchtop NMR spectroscopy with a low-cost flow-through cell design," *International Journal of Hydrogen Energy*, vol. 66, pp. 604–611, May 2024. DOI: 10.1016/j.ijhydene.2024.04.119.

[2] Z. Wang, J. Yang, Z. Li, and Y. Xiang, "Syngas composition study," *Frontiers of Energy and Power Engineering in China*, vol. 3, no. 3, pp. 369–372, Sep. 2009. DOI: 10.1007/s11708-009-0044-7.

[3] M. Herout, J. Malaťák, L. Kučera, and T. Dlabaja, "Biogas composition depending on the type of plant biomass used," *Research in Agricultural Engineering*, vol. 57, no. 4, pp. 137–143, Dec. 31, 2011. DOI: 10.17221/41/2010-RAE.

[4] L. Jin, H. Zhao, M. Wang, B. Wei, and H. Hu, "Effect of temperature and simulated coal gas composition on tar production during pyrolysis of a subbituminous coal," *Fuel*, vol. 241, pp. 1129–1137, Apr. 2019. DOI: 10.1016/j.fuel.2018.12.093.

[5] A. W. Golubkov, S. Scheikl, R. Planteu, G. Voitic, H. Wiltsche, C. Stangl, G. Fauler, A. Thaler, and V. Hacker, "Thermal runaway of commercial 18650 li-ion batteries with LFP and NCA cathodes – impact of state of charge and overcharge," *RSC Advances*, vol. 5, no. 70, pp. 57 171–57 186, 2015. DOI: 10.1039/C5RA05897J.

[6] A. W. Golubkov, D. Fuchs, J. Wagner, H. Wiltsche, C. Stangl, G. Fauler, G. Voitic, A. Thaler, and V. Hacker, "Thermal-runaway experiments on consumer li-ion batteries with metal-oxide and olivin-type cathodes," *RSC Adv.*, vol. 4, no. 7, pp. 3633–3642, 2014. DOI: 10.1039/C3RA45748F.

[7] G. Ciccarelli, J. L. Boccio, T. Ginsberg, and H. Tagawa, "The influence of initial temperature on flame acceleration and deflagration-to-detonation transition," *Twenty-Sixth Symposium (International) on Combustion/The Combustion Institute*, vol. 26, no. 2, pp. 2973–2979, 1996. DOI: 10.1016/S0082-0784(96)80140-8.

[8] K. I. Shchelkin and Y. K. Troshin, *Gasdynamics of combustion*. National Aeronautics and Space Administration, 1964, vol. 231.

[9] A. Gavrikov, A. Efimenko, and S. Dorofeev, "A model for detonation cell size prediction from chemical kinetics," *Combustion and Flame*, vol. 120, no. 1, pp. 19–33, Jan. 2000. DOI: 10.1016/S0010-2180(99)00076-0.

[10] H. D. Ng, "The effect of chemical reaction kinetics on the structure of gaseous detonations," Ph.D. dissertation, McGill University, Canada, 2005.

[11] V. Monnier, P. Vidal, V. Rodriguez, and R. Zitoun, "From graph theory and geometric probabilities to a representative width for three-dimensional detonation cells," *Combustion and Flame*, vol. 256, p. 112 996, Oct. 2023. DOI: 10.1016/j.combustflame.2023.112996.

[12] G. Bakalis, M. Valipour, J. Bentahar, L. Kadem, H. Teng, and H. D. Ng, "Detonation cell size prediction based on artificial neural networks with chemical kinetics and thermodynamic parameters," *Fuel Communications*, vol. 14, p. 100 084, Mar. 2023. DOI: 10.1016/j.jfueco.2022.100084.

[13] J. H. S. Lee, *The Detonation Phenomenon*. New York: Cambridge University Press, 2008.

[14] J. E. Shepherd, "Chemical kinetics of hydrogen-air-diluent detonations," in *Dynamics of Explosions, American Institute of Aeronautics and Astronautics*, J. R. Bowen *et al.*, Eds., vol. 106, New York: AIAA, 1986, pp. 263–293.

[15] M. Kaneshige and J. E. Shepherd, "Detonation database," GALCIT, Technical Report FM97-8, Jul. 1997, See also the electronic hypertext version at http://www.galcit.caltech.edu/detn_db/html/.

[16] G. Bakalis and H. D. Ng, "Detonation cell size prediction using artificial neural networks (ANNs) for hydrogen / hydrocarbon / ammonia / nitrous oxide mixtures," *Energies*, vol. 17, no. 7, p. 1747, Apr. 5, 2024. DOI: 10.3390/en17071747.

[17] Mechanical and Aerospace Engineering (Combustion Research). "The San Diego mechanism - version 2016-12-14 chemical-kinetic mechanisms for combustion applications," University of California, San Diego. (2016), [Online]. Available: https://web.eng.ucsd.edu/mae/groups/combustion/mechanism.html.

[18] G. P. Smith, D. M. Golden, M. Frenklach, N. W. Moriarty, B. Eiteneer, M. Goldenberg, C. T. Bowman, R. K. Hanson, S. Song, W. C. Gardiner Jr, V. V. Lissianski, and Z. Qin. "Gri-mech 3.0." GRI 3.0 Berkeley Mechanism. (1999), [Online]. Available: http://combustion.berkeley.edu/gri-mech/version30/text30.html (visited on 10/24/2023).

[19] R. Mével and J. E. Shepherd, "Ignition delay-time behind reflected shock waves of small hydrocarbons-nitrous oxide(-oxygen) mixtures," *Shock Waves*, vol. 25, pp. 217–229, 2015. DOI: 10.1007/s00193-014-0509-4.

[20] G. Blanquart, P. Pepiot-Desjardins, and H. Pitsch, "Chemical mechanism for high temperature combustion of engine relevant fuels with emphasis on soot precursors," *Combustion and Flame*, vol. 156, no. 3, pp. 588–607, 2009. DOI: 10.1016/j.combustflame.2008.12.007.

[21] S. Kao, J. Ziegler, N. Bitter, B. Schmidt, J. Lawson, and J. Shepherd, "SDToolbox: Numerical tools for shock and detonation wave modelling," CalTech, GALCIT Report FM2018.001, 2023.